Fast time-domain model for an array of interacting point-absorbers

Charitini Stavropoulou, Anders Goude, Jens Engström, and Malin Göteman

Abstract—**A fast time-domain model is developed for an array of six interacting point-absorber wave energy converters, and validated with experimental wave tank data. The devices are based on the design originated at Uppsala University. The point-absorbers move in heave and are placed in a symmetric grid, were each row contains one pair. The equations of motion are solved directly in the time domain following the Cummins' formulation. The hydrodynamic coefficients for the excitation and radiation forces are obtained using an analytical multiple-scattering method. Modelling an array of wave energy converters in time results in a system of integro-differential equations, were convolution terms appear in the excitation and radiation forces, implying that waves radiated by the body in the past continue to affect the dynamics in the future. Using time-domain models, the non-linear effects that arise during the wave energy conversion chain are treated as time-varying coefficients within the system of differential equations describing the motion. The incident waves are irregular, long-crested waves, corresponding to three different sea states. The experimental data is obtained from experiments carried out for a 1:10 scaled prototype of an array of point-absorbers. Despite the differences between the numerical and experimental set-up, the numerical model accurately captures the heaving motion of the buoys and their power absorption.**

Index Terms—**Wave power farm, point-absorber, time-domain model, in-house numerical model, fast modeling.**

I. Introduction

THE ocean covers the biggest part of the Earth's surface and is an almost boundless source of clean energy. Energy captured from the waves has a potential to fulfill the increasing worldwide demands, while helping to decrease greenhouse gas emissions [1]. Wave energy converters (WECs) are structures designed to harvest the energy in the surface waves and convert it into useful electrical energy through a power take-off (PTO) system. The wave energy industry is not yet mature, and wave energy is one of the least tapped renewable energy resources, compared to wind or solar PV [2]. To produce power more than a few MW and to enable an even power distribution, most wave energy concepts include arrays of many absorbing units, so-called wave power farms [3]. In particular, this is true for point-absorber WECs, the largest category of wave energy concepts. The WEC developed at Uppsala University [4] belongs to this category. At the ocean surface, buoys, small in relation to the wavelength, are forced to oscillate by the waves. The oscillatory motion can be converted to electricity by various methods, including hydraulic pumps or direct-driven generators.

If wave power is to become a competitive energy technology that can be realized on a large scale and contribute to the global electricity production, fundamental challenges need to be resolved. The efficiency of wave power technologies is still too low to justify large-scale implementation [5]. In a farm, the WECs interact with scattered and radiated waves which affect their dynamics and total power absorption. The performance is further affected by the electrical and mechanical subsystems [6]. To simulate, control, and optimize the behaviour of the interacting devices in various sea states, reliable numerical tools are needed. One way to solve accurately the hydrodynamic effects associated with the interaction of the ocean waves with the WEC is computational fluid dynamics (CFD) simulations, see [7] and [8]. However, due to the high computational cost associated with CFD methods, it is not suitable for control, optimisation, or farm studies.

Modelling the dynamics and performance of wave power farms is a challenging task, both numerically and experimentally. In the majority of the wave farm simulations, the equations of motion are solved in the frequency domain [9], since time-domain models are significantly more challenging to develop and computationally demanding. This is not only because of the numerical integration involved, but especially due to the computation of the convolution term accounting for the radiated water waves on the free-surface, implying that waves radiated by the body in the past continue to affect the dynamics in the future. Therefore, modelling an array of WECs in the time domain comes down to solving a system of integro-differential equations, were convolution terms appear in the computation of the excitation and radiation forces [10].

Implementing a numerical scheme to approximate the solution of such a system is not trivial, as the numerical integration involved, requires significant computational time. The effort is even heavier when more than one devices are modelled moving in many degrees of freedom. In commercial simulation tools used in studies for floats moving freely, see for instance the

This work was supported by the Swedish Research Council (grant number 2020-03634) and by STandUP for Energy. The travel costs were supported by the Åforsk scholarship fund.

Charitini Stavropoulou is PhD candidate (e-mail: charitini.stavropoulou@angstrom.uu.se); Anders Goude is Senior Lecturer/Associate Professor (e-mail: anders.goude@angstrom.uu.se); Jens Engström is Senior Lecturer/Associate Professor (e-mail: jens.engstrom@angstrom.uu.se); Malin Göteman is Associate Professor; and deputy director of the Centre of Natural Hazards and Disaster Science (CNDS), Sweden. (e-mail: malin.goteman@angstrom.uu.se). All authors are at the Department of Electrical Engineering, Uppsala University. Lägerhyddsvägen 1, 752 37, Uppsala Sweden.

Digital Object Identifier:
https://doi.org/10.36688/ewtec-2023-265

open-source software WEC-Sim in [11], a lot of effort has been put to substitute the convolution integral in the radiation force. The replacement is done by a set of coupled linear Ordinary Differential Equations (ODEs), usually expressed in a matrix form, and this way an extra number of states is added to the existed formulation. This so-called state-space representation is more efficient due to its Markovian property, at any instant, the value of the state summarises all the past system information [12].

In this work, we model an array of six interacting point-absorber WECs using a time-domain formulation, where no substitution is assumed for the convolution term in the radiation force. Instead the numerical integration involved is performed directly. The mathematical and numerical procedure will be explained in detail, as we have found this to be seldom included in publications, and to enable reproducibility of the results. A unique feature of the developed time-domain model is that the validation is done with actual experimental data. Such data for wave power farms is rare, due to the complexity and costs associated with the task. The experimental results we use were carried out in the COAST Lab at Plymouth University, UK, corresponding to a 1:10 scaled prototype of an array of point-absorbers [13].

The rest of the paper is organised as follows. In Section II the theoretical background is presented. In Section III the simulation results are compared against the experimental data, and in Sections IV and V the main results are discussed.

II. Theory and method

We consider an array of N interacting point-absorbers moving in one degree of freedom, heave. In the rest of this work, all the hydrodynamic coefficients correspond to the heaving mode. The equations of motion for the floating bodies can be described by the following system of ODEs,

$$\begin{aligned}\big(M_b + M^{add}(\infty)\big)\cdot \ddot{z}_b(t) = \\ F_e(t) + F_r(t) + F_h(t) + F_l(t) - W_b.\end{aligned} \tag{1}$$

Here M_b is the diagonal matrix containing the masses of the floating buoys m_{b_j}, where $j = 1, ..., N$ and $M^{add}(\infty)$ is the matrix containing the added masses at the infinite frequency limit. The added mass matrix at the infinite frequency contains inputs $m^{add}_{ij}(\infty)$ for each pair ij of interacting point-absorbers, where $i, j = 1, ..., N$. The solution vector, denoting the vertical displacement of the buoys is $z_b(t) = (z_{b_1}(t), ..., z_{b_N}(t))^T$. The excitation force is $F_e(t) = (F_{e_1}(t), ..., F_{e_N}(t))^T$ and the radiation force is $F_r(t) = (F_{r_1}(t), ..., F_{r_N}(t))^T$. Similarly, $F_h(t)$ is the hydrostatic buoyancy force, $F_l(t)$ is the force from the mooring line, connecting the surface buoy to the translator inside the generator, and W_b is the vector containing the weights of the buoys.

A. The radiation force

Under the assumption of linear potential flow theory, the fluid is assumed to be non-viscous, irrotational and incompressible, the waves are non-steep and the boundary conditions are linearised. Then, the fluid-structure interaction problem can be solved using a linear hydrodynamic formulation, also for large farms and control applications.

The radiation force in the Cummins' formulation (1) is a result of the radiation property of water waves. In the time domain, the inverse Fourier transform of the radiation force is [14],

$$F_{rad}(t) = F_r(t) - M^{add}(\infty)\ddot{z}_b(t), \tag{2}$$

where

$$F_r(t) = -k(t) * \dot{z}_b(t). \tag{3}$$

Eqs. (2) and (3) are analogous to the radiation terms we have introduced in Eq. (1), where the infinite mass, integrated within the radiation force, is extracted to ensure convergence at infinity. Further, $k(t)$ is the radiation impulse response function (RIRF), or memory function, physically representing the effect of the past body oscillations on its actual state [10]. Since the RIRF is a real and causal function ($k(t) = 0$ and $t < 0$), it is enough to know either the radiation damping coefficient $R(\omega)$ or the added mass to derive it [14],

$$k(t) = \frac{2}{\pi}\int_0^\infty R(\omega)\cos(\omega t)\,\mathrm{d}\omega. \tag{4}$$

To compute the convolution integral in Eq. (3) we take into consideration the causality of the RIRF and the commutativity of the convolution product. If we further assume that the velocity input is causal as well, then the convolution term becomes

$$F_r(t) = -k(t) * \dot{z}_b(t) = -\int_0^t k(t-\tau)\dot{z}_b(\tau)\,\mathrm{d}\tau. \tag{5}$$

One of the difficulties in the computation of the radiation force is the accurate numerical approximation of the RIRF. To compute the integral in Eq. (4) over a finite frequency range we have to introduce an upper truncation limit, which should be sufficiently high to achieve an accurate numerical evaluation [15]. The radiation damping tends to zero at the infinite frequency limit, hence it is sufficient to introduce an upper frequency value for this coefficient to be negligible. Taking as the truncation frequency the one above which $R(\omega)$ is less than one thousandth its maximum value produces satisfactory accuracy [10], [16]. In this work we use the analytical multiple-scattering model of [17] to compute the radiation damping $R(\omega)$ and the added mass $M^{add}(\omega)$ in the frequency domain. The analytical model for determining the hydrodynamic coefficients is exact within the limitations of linear potential flow theory and we are able to choose the desired upper truncation frequency limit $\Omega = 16$ rad/s,

$$k(t) = \frac{2}{\pi}\int_0^\Omega R(\omega)\cos(\omega t)\,\mathrm{d}\omega. \tag{6}$$

The numerical integration of Eq. (6) can be achieved under proper handling. The direct application of the trapezoidal method can generate a periodic function with period equal to the inverse of the frequency spacing $2\pi/d\omega$, which is a pure numerical artefact [10]. In reality the RIRF has a decaying behaviour, affecting the

buoy velocity in the convolution term only for a few seconds. To avoid the periodic occurrence we define the RIRF in a time interval that is smaller than the inverse of half of the frequency spacing. Using a small enough frequency step $d\omega$, we interpolate the radiation damping for finer frequency resolution, then we can create a time-varying RIRF with high period. This method ensures accuracy in the RIRF implementation, as the repeated occurrence would appear much later. Due to the rapid RIRF decay, a time stamp t_{decay} can be set, after which the RIRF influence in negligible [10]. The Cummins' formulation in Eq. (1) becomes

$$\begin{aligned}\big(M_b + M^{add}(\infty)\big) \cdot \ddot{z}_b(t) = \\ F_e(t) - \int_0^t k(t-\tau)\dot{z}_b(\tau)\,\mathrm{d}\tau + F_h(t) + F_l(t) - W_b.\end{aligned} \tag{7}$$

The major difficulty in the numerical approximation of Eq. (7) is the computation of the convolution integral in the radiation force. The numerical integration requires significant computational effort, since large amount of data need to be stored to evaluate the integral in every time-step. The effort is even heavier when more than one devices are modelled moving in many degrees of freedom. One common approach to solve this is to apply the state-space formulation [11]. In this work, we instead employ a direct integration, made computationally feasible by the constraint that the buoys are moving only in heave. We denote the convolution integral in Eq. (5) as $I(t)$. Since the influence of $I(t)$ is limited after the specified time t_{decay}, we obtain,

$$I(t) = \int_0^t k(t-\tau)\dot{z}_b(\tau)\mathrm{d}\tau \approx \int_0^{t_{decay}} k(\tau)\dot{z}_b(t-\tau)\,\mathrm{d}\tau. \tag{8}$$

At each time instant t, the convolution integral describes the area under $\dot{z}_b(\tau)$ weighted by $k(t-\tau)$. As t changes, the weighting function $k(t-\tau)$ emphasises different parts of the velocity history $\dot{z}_b(\tau)$. For computational efficiency the RIRF is not required to be computed at every time-step during the numerical integration of Eq. (7). A vector of pre-computed values of the RIRF can be used together with the velocity history [15]. To compute the integral in Eq. (8) we can apply the trapezoidal method, assuming that the numerical method used for the solution of the ODE system in Eq. (7) has a constant time step dt. For every pair of interacting floating bodies ij each element within the integral vector $I(t)$ is approximated as

$$\begin{aligned}I_j(t) \approx \sum_{i=1}^{N} \Bigg(\frac{k_{ij}(0)\dot{z}_{b_j}(t) + k_{ij}(t)\dot{z}_{b_j}(t-t_{decay})}{2} \\ + \sum_{n=1}^{L-1} k_{ij}(ndt)\dot{z}_{b_j}(t-n\,\mathrm{d}t)\Bigg).\end{aligned} \tag{9}$$

Since we are implementing an array of six floats, moving in heave, the inputs to the RIRF array $k(t)$ are denoted as $k_{ij}(t)$ for every pair ij of interacting point-absorbers. At every time-step, the length of the summation vector is $L = t_{decay}/\,\mathrm{d}t$, as for each float, L data points corresponding to the previous values of the velocity history have to be stored and used in $\mathcal{O}(L)$ arithmetic operations including products and sums.

B. The excitation force

The excitation force $F_e(t)$ is the dominant force from the incoming wave. In the time domain, the force is given by

$$F_e(t) = f_e(t) * a(t) = \int_{-\infty}^{\infty} f_e(\tau)a(t-\tau)\,\mathrm{d}\tau. \tag{10}$$

Here, $a(t)$ is the wave elevation at a point of reference O on the free surface with coordinates (x_0, y_0) and $f_e(t)$ is the excitation impulse response function (IRF) [14]. In contrast to the RIRF, the excitation IRF is not necessarily causal. Hence, future knowledge of the surface elevation is necessary to compute the current excitation force. Several approaches to predict the incoming wave within limited time horizons exist, see [18]–[21]. Here, we make the simplified assumption that the incoming wave is known over the time range we wish to solve the Cummins' formulation, which makes the numerical implementation of Eq. (10) straight-forward.

C. Buoy configuration

We are interested to compare the numerical results regarding the motion and the power absorption of the interacting buoys against experimental data. The physical experiments are carried out at a 1:10 scale and consider an array of six identical point-absorbers, free to move in six degrees of freedom. The surface buoys are ellipsoids with radius $R_{exp} = 0.244$ m and draft $d_{exp} = 0.0948$ m, and they are connected to six individual power take-off (PTO) systems. The array layout studied is a symmetric grid, with one pair of floats in each row; a detailed discussion on the different array configurations used in the experiments can be found in [13]. In the numerical implementation, the geometry of each buoy consists of a cylinder with radius $R_{cyl} = 0.178$ m and draft $d_{cyl} = 0.0948$ m, which corresponds to the same submerged volume and draft of the physical elliptical buoys. This is because the analytical multiple-scattering model of [17] used to compute the hydrodynamic coefficients for the excitation and radiation forces can only handle cylinder-shaped floats or cylinders with moon-pool. To compute the buoyancy force vector $F_h(t)$ in the Cummins' formulation we use the Archimedes' principle as

$$F_h(t) = \rho g \pi R_{cyl}^2 (d_{cyl} - z_b(t)), \tag{11}$$

where $g = 9.81$ m/s^2 is the acceleration due to gravity, and $\rho = 1000$ kg/m^3 is the water density.

D. PTO configuration

In the physical experiments, an alternating rotatory generator is used as a PTO system; a detailed discussion can be found in [22]. The PTO dynamics are described by the system of ODEs,

$$M_t \cdot \ddot{z}_t(t) = F_{PTO}(t) + F_l'(t) - W_t. \tag{12}$$

Here, M_t is the diagonal matrix containing the mass of each translator and $z_t(t) = (z_{t_1}(t), ..., z_{t_N}(t))^T$ is the solution vector describing the vertical displacement. $F_l'(t)$ is the mooring line force acting on the translator and

W_t is the vector containing the weights. We model each point-absorber as one body, assuming a stiff connection line between the surface buoy and the translator. This way, the coupled system (7)–(12) is replaced by one equation of motion as

$$\begin{aligned}\left(M_b + M_t + M^{add}(\infty)\right) \cdot \ddot{z}(t) = \\ F_e(t) - \int_0^t k(t-\tau)\dot{z}(\tau)\,\mathrm{d}\tau + F_h(t) + \\ F_{PTO}(t) - (W_b + W_t).\end{aligned} \tag{13}$$

The damping force from the PTO system is given as

$$F_{PTO}(t) = -\gamma \dot{z}(t). \tag{14}$$

For the damping coefficient γ, a constant value of 306 Ns/m is used, together with an additional damping of 63.2 Ns/m to account for the rope friction, see [13].

E. Numerical model

Eq. (13) is a system of integro-differential equations. Therefore we can apply a fixed-step, explicit, Runge-Kutta 4th order scheme (RK4) with time step $\mathrm{d}t = 0.05$ s. This integration method is quite fast providing a balance between accuracy of the results and computational efficiency. Although a more efficient integration would involve variable-step routines, in our case a fixed-step solver is more suitable. That is due to the trapezoidal method involved in the computation of the convolution term in the radiation force. A constant time step within the integration routine will ensure that the computation of the radiation integral in Eq. (9) and the RIRF are consistent during the whole simulation. The r_{th} stage explicit Runge-Kutta method for Eq. (13) is defined as follows,

$$\begin{aligned} z_{n+1} &= z_n + \mathrm{d}t(b_1 k_1 + b_2 k_2 + ... + b_r k_r), \\ t_{n+1} &= t_n + \mathrm{d}t. \end{aligned} \tag{15}$$

Here, $n = 1, ..., T$, where T accounts for the end in the wave time series. The coefficients b_i are obtained from the Butcher tableau of the classic 4th order Runge Kutta method and the weights k_i are recursively obtained by solving a linear system at each time step. The simulation is performed in MATLAB.

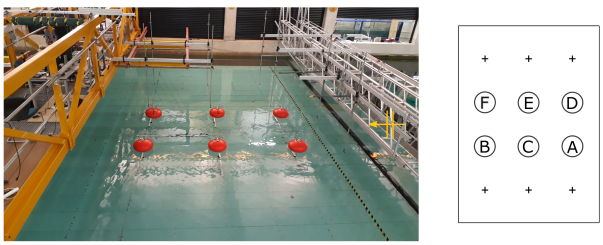

Fig. 1. Layout of the experimental array configuration of the interacting point-absorbers. Illustration is taken by [13].

F. Physical experiment

The experiments were carried out in 2018 in the COAST Lab at Plymouth University, UK. The specific results we use in this work correspond to an array of six devices placed in a symmetric grid, with one pair in each row. The model represents a 1:10 scaled prototype of an array of point-absorbers, based on the WEC concept developed at Uppsala University. The physical set-up consists of six, identical, elliptical buoys moving freely in six degrees of freedom. The PTO system is located above the water connected to the buoys via ropes, see [13] and [22]. The WEC array geometry can be seen in Fig. 1.

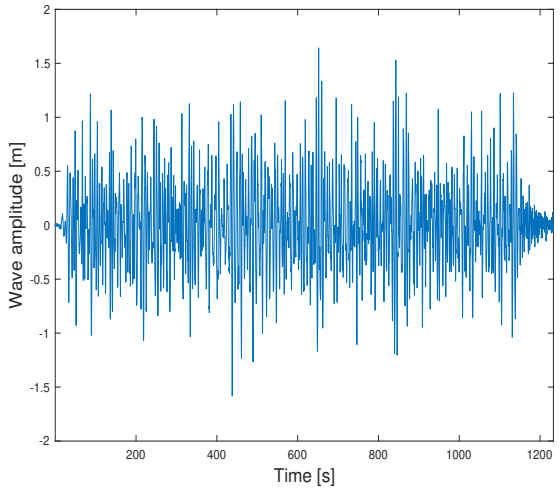

Fig. 2. Irregular wave (IW3), generated through the Bretschneider spectrum. The significant wave height is H_s = 1.75 m, and the energy period is T_e = 6.5 s.

TABLE I
INCIDENT WAVES.

	1 : 10			1 : 1		
Wave ID	H_s[m]	T_e[s]	T[min]	H_s[m]	T_e[s]	T[min]
IW1	0.175	1.42	6	1.75	4.5	20
IW2	0.175	1.74	6	1.75	5.5	20
IW3	0.175	2.06	6	1.75	6.5	20

[a] Irregular waves corresponding to three sea states and the full scale (1:1) components used in the numerical simulation. Table information is taken by [13].
[b] The irregular waves are characterized by the significant wave height H_s and the energy period T_e. The total wave time is denoted as T. Table information is taken by [13].

TABLE II
WEC AND SYSTEM SPECIFICATIONS

Parameters	Symbol	Units	1 : 10	1 : 1
Exp. buoy radius	R_{exp}	[m]	0.244	2.44
Exp. buoy draft	d_{exp}	[m]	0.0948	0.948
Cyl. buoy radius	R_{cyl}	[m]	0.178	1.78
Cyl. buoy draft	d_{cyl}	[m]	0.0948	0.948
Damping	γ	[Ns/m]	306	$9.68 \cdot 10^4$
Water depth	h	[m]	2.5	25

The experimental (Exp.) and the numerical (Cyl.) radii and draft. The generator damping is denoted as γ and the water depth as h. Froude scaling is used to derive the full scale components. Table information is taken by [13].

III. Results

To study whether the linear model simulates accurately the heaving motion and the power absorption of each of the interacting devices within the array configuration, despite the simplifying assumptions made, we compare the numerical results against the experimental data described above. The dynamics of the WECs as well as the absorbed power are compared in Sections III-A and III-B, respectively.

A. WEC dynamics

The response of the WECs is tested in three different sea states represented by irregular waves obtained from the Bretschneider spectrum. Detailed information on the sea states and the parameters used in the experiments and the numerical simulations can be found in Tables I and II. We study the simulated and the experimental peak and trough buoy motion $z(t)$, calculated according to wave peaks and troughs obtained during each wave period i. To compare the numerical and experimental results, we use both linear fitting and an error metric defined as

$$\text{Error}_z = \text{average}\left\{\frac{\left|z^{(i)\text{exp}}_{\text{peak,trough}} - z^{(i)\text{sim}}_{\text{peak,trough}}\right|}{\left|z^{(i)\text{exp}}_{\text{peak,trough}}\right|}\right\}. \quad (16)$$

The comparison is performed for each WEC within the array, and for each irregular wave in Table I. The numerical results were run in full scale, and compared with the experimental data using Froude scaling. In Figs. 3–5, the time series of the buoy elevation, for the last irregular wave (IW3), are shown for the first row of WECs A and D, towards the incoming wave, the middle row C, E, and the last row of WECs, B and F. The numerical buoy motion follows the experimental data quite well, especially for the first row of devices. This phenomenon is expected as in the middle and last row within the grid, the non-linear effects due to the intense hydrodynamic interaction are increasing. Further, the numerical and experimental motion peaks for each WEC are shown in Figs. 6–11 together with the linear fitting. The best agreement between the numerical and the experimental peaks is for the first row of WECs A, D. However, the middle and the last row C, E and B, F are following the linear trend as well, showing acceptable agreement between the numerical and the experimental data, especially for the smallest wave peaks. Since the motion analysis has been performed for peaks and troughs for each WEC and for each irregular wave, in Figs. 12 and 13 we can see a combined plot of the peak and trough motion error percentage according to Eq. (16). The average motion error varies for each WEC and for each irregular wave. The average peak error is typically less for the first row of WECs A and D, and is increasing towards the upper back part of the grid. The average trough error is also typically less for WECs A and D.

B. Absorbed power

We compare the average power absorption for each WEC and for the whole park, for each irregular wave in Table I. The computed and measured power are shown in Figs. 14–17. The results are relatively similar for the three irregular waves. Regarding the individual devices, the best match between the numerical and the experimental results are for the most front row of devices.

IV. Discussion

In this study, we have developed a linear time-domain model to simulate the motion of each wave energy converter (WEC) within an array configuration, taking into account the complex hydrodynamics arising from the interaction with scattered and radiated waves. The performance of the WECs has been evaluated for three different sea states represented by the irregular waves listed in Table I.

A key aspect of this study is the validation of the heaving motion and power absorption of each WEC using experimental data obtained from a 1:10 scaled prototype of an array of point-absorbers. In Figs. 3–5, we present the time series of the buoy elevation for each row of devices within the array, focusing on the irregular wave IW3. Despite the presence of irregular waves and the inherent non-linear phenomena involved, the numerical buoy motion closely matches the experimental data. The validation is further supported by analyzing peaks and troughs for each wave period, as illustrated in Figs. 6–11 and Figs. 12–13. Notably, the front row of WECs (A and D) exhibits the least average motion error, as the numerical and experimental motion peaks align well with the linear fit. This observation aligns with expectations, as the non-linear hydrodynamic interactions become more pronounced deeper within the array configuration (WECs C, E, B, and F), making the accurate capture of heaving motion for the middle and back rows more challenging using a linear numerical scheme.

Further, we analyze the average power absorption for each WEC within the array and for all the examined irregular waves. From Figs. 14–16 it is shown that the results demonstrate consistent behavior for all wave scenarios. Similar to the motion results, the best agreement between the experimental and numerical results is generally observed for the front row of devices (A and D). Fig. 17 depicts the comparison of the average power absorption for the entire wave power farm, showing good agreement between the numerical and experimental data. It is important to note that despite the percentage differences between the numerical and the experimental peaks and troughs (as seen in Figs. 12–13), the resulting absorbed power shows a high level of agreement (as seen in Figs. 14–17). The linear scheme can capture the general trend of the motion, it cannot simulate in detail the extreme peaks or troughs. Although the heave motion experiences occasional, instantaneous peaks, these fluctuations do not substantially contribute to the power absorption. Therefore, the numerical model developed in this study is capable of rapidly providing a reliable estimate of the power absorption for the wave power farm.

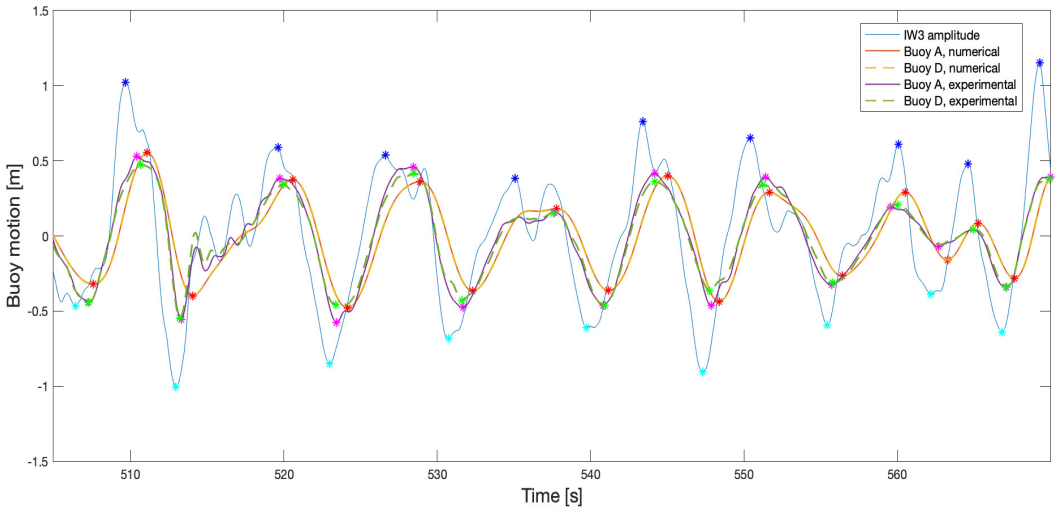

Fig. 3. Time series of the buoy elevation for the first row of WECs, A and D, together with the according experimental data. The markers in the plot correspond to peaks and troughs used in the validation of the scheme. The incoming wave corresponds to irregular wave IW3.

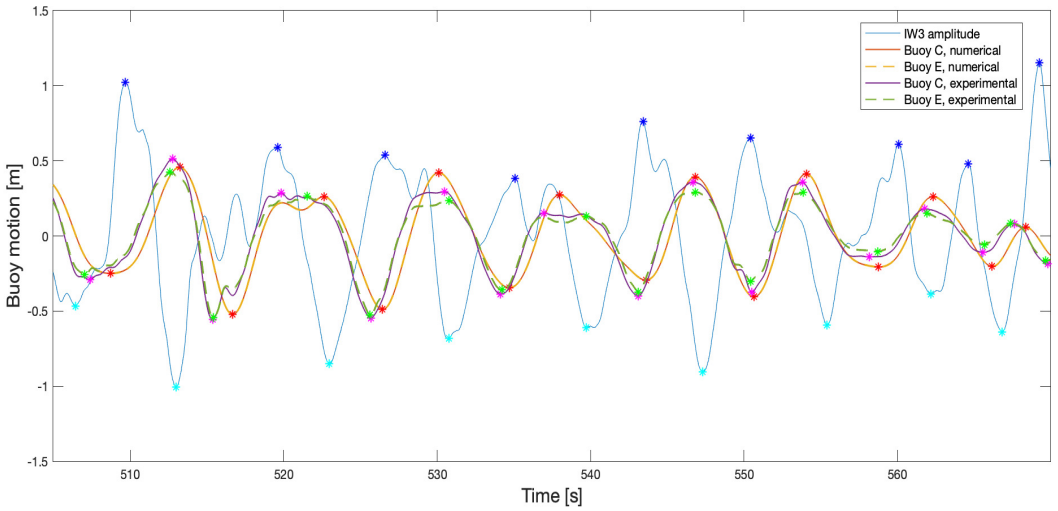

Fig. 4. Time series of the buoy elevation for the middle row of WECs, C and E, together with the according experimental data. The markers in the plot correspond to peaks and troughs used in the validation of the scheme. The incoming wave corresponds to irregular wave IW3.

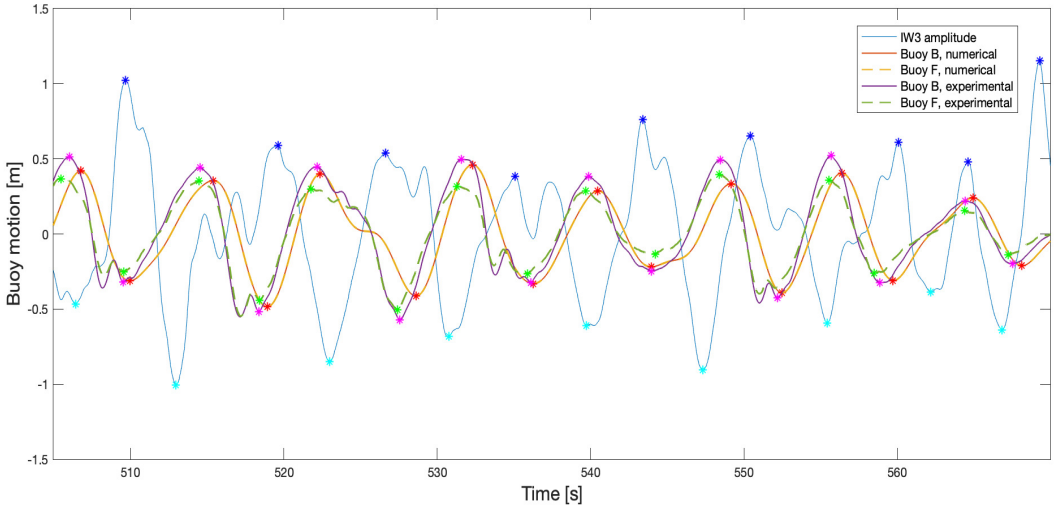

Fig. 5. Time series of the buoy elevation for the last row of WECs, B and F, together with the according experimental data. The markers in the plot correspond to peaks and troughs used in the validation of the scheme. The incoming wave corresponds to irregular wave IW3.

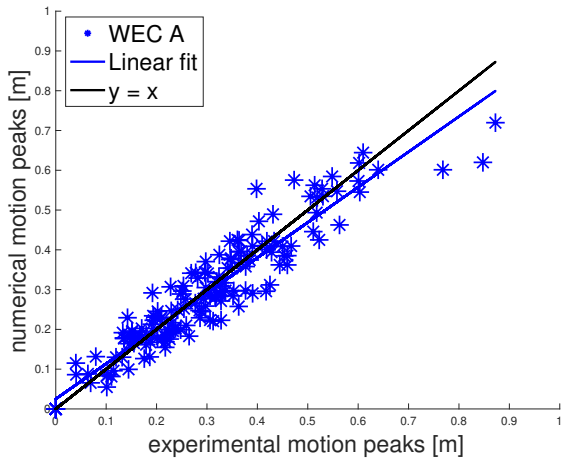

Fig. 6. Numerical peaks plotted against experimental peaks, together with a linear fitting for WEC A and irregular wave IW3.

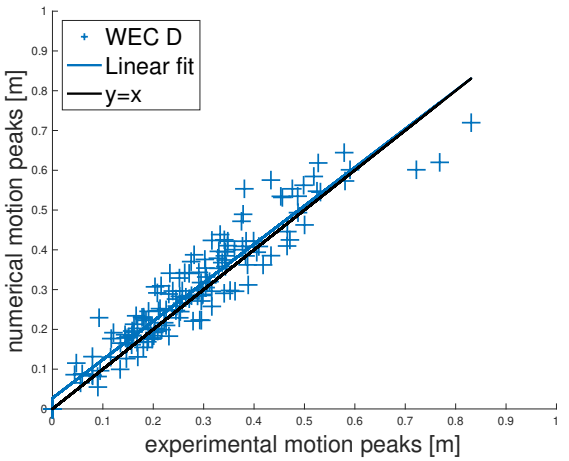

Fig. 9. Numerical peaks plotted against experimental peaks, together with a linear fitting for WEC D and irregular wave IW3.

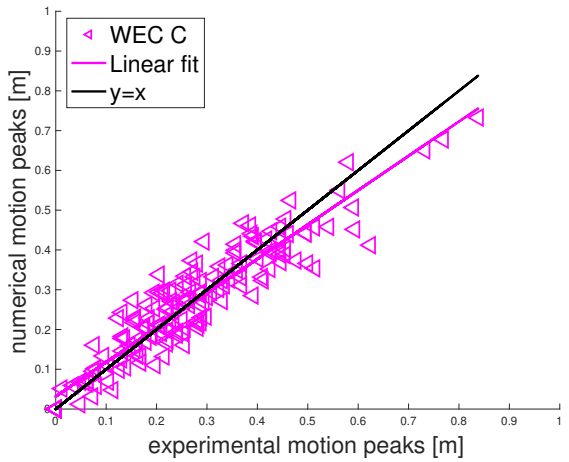

Fig. 7. Numerical peaks plotted against experimental peaks, together with a linear fitting for WEC C and irregular wave IW3.

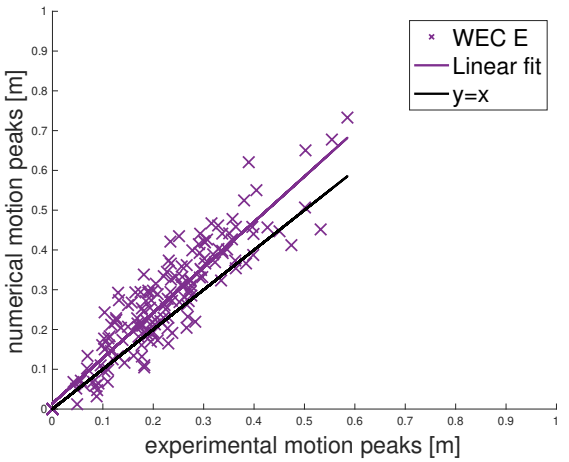

Fig. 10. Numerical peaks plotted against experimental peaks, together with a linear fitting for WEC E and irregular wave IW3.

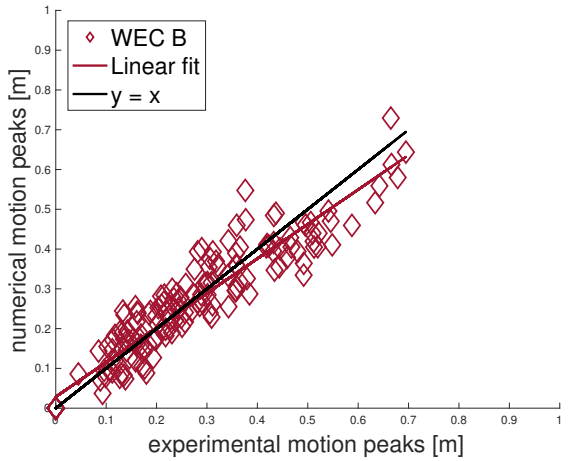

Fig. 8. Numerical peaks plotted against experimental peaks, together with a linear fitting for WEC B and irregular wave IW3.

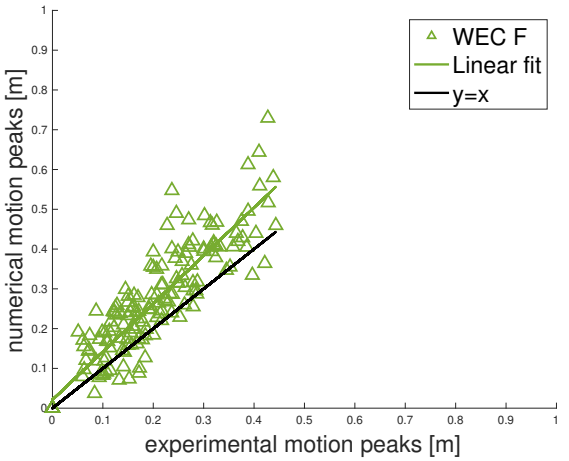

Fig. 11. Numerical peaks plotted against experimental peaks, together with a linear fitting for WEC F and irregular wave IW3.

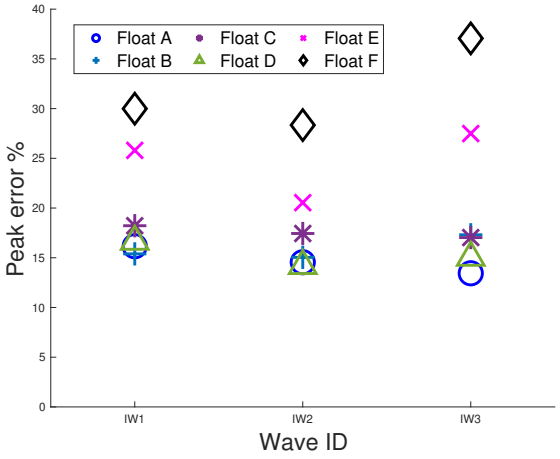

Fig. 12. Graph of the average peak error percentage for each WEC within the array configuration and for each irregular wave in Table I.

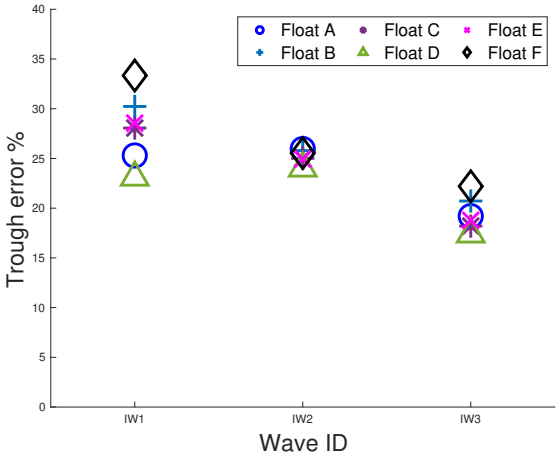

Fig. 13. Graph of the average trough error percentage for each WEC within the array configuration and for each irregular wave in Table I.

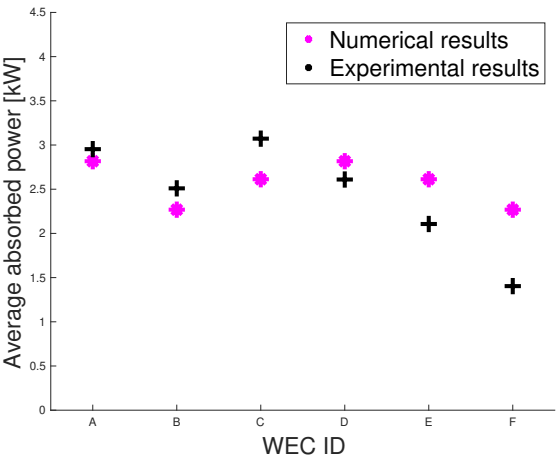

Fig. 14. Graph of the average power absorption for each WEC for the first irregular wave IW1.

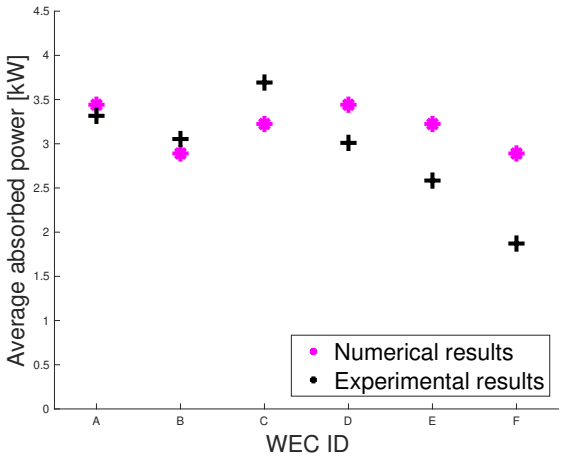

Fig. 15. Graph of the average power absorption for each WEC for the second irregular wave IW2.

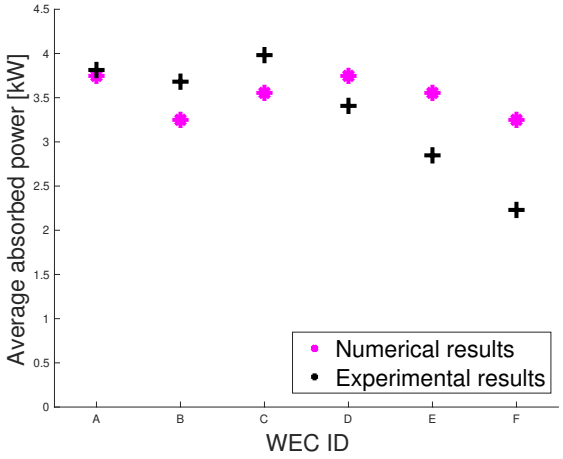

Fig. 16. Graph of the average power absorption for each WEC for the third irregular wave IW3.

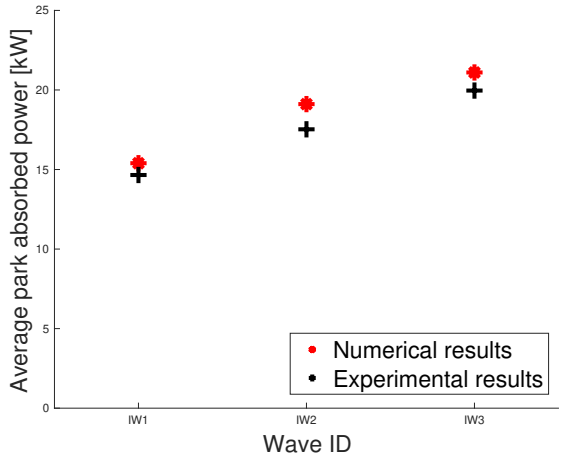

Fig. 17. Graph of the average park power absorption for each irregular wave in Table I.

V. Conclusions

In this work, we have presented a numerical model to simulate the motion and power absorption of an array of interacting point-absorber wave energy converters (WECs), inspired by the design originated at Uppsala University. The devices undergo heave motion, and their response is tested using three irregular waves generated from the Bretschneider spectrum. Our simulation approach involves an in-house, time-domain model that employs direct numerical integration to solve the system of integro-differential equations governing the WECs' behavior.

We emphasize that the strength of our model lies in its simplicity and efficiency. It is a fast and linear tool that demands minimal computational effort for accurately modeling the motion and power output of a wave power farm. To achieve even higher accuracy, more sophisticated high-fidelity models, as highlighted in [23], should be employed. However, due to the significant computational cost associated with such models, low- or mid-fidelity models like the one presented in this study remain the only viable option for analyzing arrays of interacting devices.

A unique aspect of this work is the validation of our numerical scheme using actual experimental data. Acquiring such data is often challenging, particularly in the context of arrays of interacting units, making our results noteworthy. The physical setup used for validation represents a 1:10 scaled prototype of a point-absorber array comprising six identical buoys capable of free motion in six degrees of freedom. Despite the disparity between the irregular wave environment employed in the experiments and the numerical simulations, our linear model accurately captures the heaving motion of the devices. Notably, the front row of WECs, facing the incoming waves, generally exhibits the least average motion error, while the non-linear effects become more pronounced deeper within the array. We calculate the absorbed power for both individual WECs and the entire farm based on the motion data, and our numerical results show good agreement with the experimental findings.

Acknowledgement

We would like to thank Eirini Katsidoniotaki, Postdoctoral Researcher at MIT, for her valuable insights, comments, and feedback on this work. Her input has significantly enhanced the quality and clarity of our research.

References

[1] T. H. Soukissian, D. Denaxa, F. Karathanasi, A. Prospathopoulos, K. Sarantakos, A. Iona, K. Georgantas, and S. Mavrakos, "Marine renewable energy in the mediterranean sea: Status and perspectives," *Energies*, vol. 10, no. 10, 2017. [Online]. Available: https://www.mdpi.com/1996-1073/10/10/1512

[2] A. Maria-Arenas, A. J. Garrido, E. Rusu, and I. Garrido, "Control strategies applied to wave energy converters: State of the art," *Energies*, vol. 12, no. 16, p. 3115, 2019.

[3] M. Göteman, M. Giassi, J. Engström, and J. Isberg, "Advances and challenges in wave energy park optimization—a review," *Frontiers in Energy Research*, vol. 8, 2020. [Online]. Available: https://www.frontiersin.org/articles/10.3389/fenrg.2020.00026

[4] M. Leijon *et al.*, "Wave energy from the North Sea: Experiences from the Lysekil research site," *Surveys in geophysics*, vol. 29, no. 3, pp. 221–240, 2008.

[5] E. Rusu and F. Onea, "A review of the technologies for wave energy extraction," *Clean Energy*, vol. 2, no. 1, pp. 10–19, 2018.

[6] M. Göteman, C. McNatt, M. Giassi, J. Engström, and J. Isberg, "Arrays of point-absorbing wave energy converters in short-crested irregular waves," *Energies*, vol. 11, no. 4, 2018. [Online]. Available: https://www.mdpi.com/1996-1073/11/4/964

[7] E. Katsidoniotaki, E. Nilsson, A. Rutgersson, J. Engström, and M. Göteman, "Response of point-absorbing wave energy conversion system in 50-years return period extreme focused waves," *Journal of Marine Science and Engineering*, vol. 9, no. 3, p. 345, 2021.

[8] E. Katsidoniotaki and M. Göteman, "Numerical modeling of extreme wave interaction with point-absorber using openfoam," *Ocean Engineering*, vol. 245, p. 110268, 2022. [Online]. Available: https://www.sciencedirect.com/science/article/pii/S0029801821015754

[9] M. Göteman, "Optimisation of wave farms," in *Modelling and Optimization of Wave Energy Converters* :. CRS Press, 2022, pp. 281–308.

[10] P. Ricci, "Chapter 3 - time-domain models," in *Numerical Modelling of Wave Energy Converters*, M. Folley, Ed. Academic Press, 2016, pp. 31–66. [Online]. Available: https://www.sciencedirect.com/science/article/pii/B9780128032107000037

[11] Y.-H. Yu, M. Lawson, K. Ruehl, and C. Michelén Ströfer, "Development and demonstration of the wec-sim wave energy converter simulation tool," 01 2014.

[12] Z. Yu and J. Falnes, "State-space modelling of a vertical cylinder in heave," *Applied Ocean Research*, vol. 17, no. 5, pp. 265–275, 1995. [Online]. Available: https://www.sciencedirect.com/science/article/pii/0141118796000028

[13] M. Giassi, J. Engström, J. Isberg, and M. Göteman, "Comparison of wave energy park layouts by experimental and numerical methods," *Journal of Marine Science and Engineering*, vol. 8, 09 2020.

[14] J. Falnes, *Ocean Waves and Oscillating Systems: Linear Interactions Including Wave-Energy Extraction*. Cambridge University Press, 2002.

[15] A. Kurniawan, J. Todalshaug, and T. Moan, "Assessment of time-domain models of wave energy conversion systems," 09 2011.

[16] P. Ricci, J.-B. Saulnier, A. Falcão, and M. Pontes, "Time-domain models and wave energy converters performance assessment," vol. 6, 01 2008.

[17] M. Göteman, J. Engström, M. Eriksson, and J. Isberg, "Fast modeling of large wave energy farms using interaction distance cut-off," *Energies*, vol. 8, pp. 13 741–13 757, 12 2015.

[18] F. Fusco and J. V. Ringwood, "A study of the prediction requirements in real-time control of wave energy converters," *IEEE Transactions on Sustainable Energy*, vol. 3, no. 1, pp. 176–184, 2011.

[19] A. A. E. Price, D. I. Forehand, and A. R. Wallace, "Time-span of future information necessary for theoretical acausal optimal control of wave energy converters," in *2009 European Control Conference (ECC)*. IEEE, 2009, pp. 3761–3766.

[20] M. P. Schoen, J. Hals, and T. Moan, "Wave prediction and robust control of heaving wave energy devices for irregular waves," *IEEE Transactions on energy conversion*, vol. 26, no. 2, pp. 627–638, 2011.

[21] Z. Shahroozi, M. Göteman, J. Engström, and J. H. Todalshaug, "Considerations on prediction horizon and dissipative losses for wave energy converters," *IET Renewable Power Generation*, vol. 15, no. 14, pp. 3434–3458, 2021.

[22] S. Thomas, M. Giassi, M. Göteman, M. Hann, E. Ransley, J. Isberg, and J. Engström, "Performance of a direct-driven wave energy point absorber with high inertia rotatory power take-off," *Energies*, vol. 11, p. 2332, 09 2018.

[23] E. Katsidoniotaki, Z. Shahroozi, C. Eskilsson, J. Palm, J. Engström, and M. Göteman, "Validation of a CFD model for wave energy system dynamics in extreme waves," *Ocean Engineering*, vol. 268, p. 113320, 2023.